Journal of The Electrochemical Society, **155** (11) B1179-B1183 (2008)
0013-4651/2008/155(11)/B1179/5/$23.00 © The Electrochemical Society

SOFC Anodes Based on Infiltration of $La_{0.3}Sr_{0.7}TiO_3$

Shiwoo Lee,[a,b] Guntae Kim,[a] J. M. Vohs,[a,*] and R. J. Gorte[a,*,z]

[a]*Department of Chemical and Biomolecular Engineering, University of Pennsylvania, Philadelphia, Pennsylvania 19104, USA*
[b]*Korea Institute of Energy Research, Daejeon 305-343, Korea*

Composites formed by infiltration of 45 wt % $La_{0.3}Sr_{0.7}TiO_3$ (LST) into 65% porous yttria-stabilized zirconia (YSZ) were examined for application as solid oxide fuel cell (SOFC) anodes. Although LST does not react with YSZ, the structure of the LST deposits was strongly affected by the calcination temperature. At 1373 K, the LST formed loosely packed, 0.1 μm particles that filled the YSZ pores. The conductivity of this composite depended strongly on the pretreatment conditions but was greater than 0.4 S/cm after heating to 1173 K in humidified (3% H_2O) H_2. Following calcination at 1573 K, the LST had sintered significantly, decreasing the conductivity of the composite by a factor of approximately 5. The addition of a catalyst was critical for achieving reasonable electrochemical performance, with the addition of 0.5 wt % Pd and 5 wt % ceria increasing the power density of otherwise identical cells from less than 20 to 780 mW/cm^2 for operation in humidified (3% H_2O) H_2 at 1073 K. Electrodes prepared from LST deposits calcined at 1373 K were found to exhibit a much better performance than those prepared from LST deposits calcined at 1573 K, demonstrating that the structure of the composite is critical for achieving high performance.
 [DOI: 10.1149/1.2976775]

Manuscript submitted June 12, 2008; revised manuscript received July 22, 2008. Published September 22, 2008.

Increased efficiency for the conversion of chemical energy to electrical energy is going to be very important for many applications in the future. Because of this, solid oxide fuel cells (SOFCs) are attractive for the intrinsically high efficiency they exhibit. This efficiency derives in part from their high operating temperatures (between 873 and 1073 K), which decrease electrode overpotentials compared to that found with other types of fuel cells. (The electrode overpotential is defined as the difference between the ideal Nernst potential and the actual electrode potential.) Equally important, SOFCs are "fuel" flexible, partly because of their high operating temperatures but also because the electrolytes are oxygen-ion conductors rather than proton conductors. In principle, any combustible fuel can react with the oxygen ions to produce electrons.[1]

However, to take full advantage of the intrinsic fuel flexibility, it is necessary that the material used for the anode be stable in the combustible fuel. For SOFCs with yttria-stabilized zirconia (YSZ) electrolytes, the state-of-the-art anode is a mixture of YSZ with Ni, usually referred to as a ceramic–metallic (cermet) composite.[2] Ni–YSZ cermets perform very well under some conditions but have several important limitations. First, the cermets are not stable to reoxidation. Second, Ni-based electrodes cannot be exposed to hydrocarbon fuels unless sufficient steam is present to prevent Ni from catalyzing the formation of carbon fibers, especially with hydrocarbons larger than methane.[1] Carbon-fiber formation is a serious problem because it can destroy the electrode by loss of Ni due to metal dusting[3] and by producing stresses within the electrode that can fracture the cell.[4] Carbon formation in the presence of dry hydrocarbons can be avoided by replacing Ni with a metal that does not catalyze fiber formation, like Cu,[5] but the thermal stability of alternative electrodes tends to be worse.[6,7]

Electrodes based on conducting ceramics could provide an almost ideal solution to the problems associated with Ni–YSZ cermets if the ceramic electrodes could provide comparably low electrode losses.[8] Oxides would not be expected to catalyze the formation of carbon fibers the way that Ni does because carbon dissolution is a key step in the formation of carbon fibers on Ni, and oxides do not dissolve carbon.[1,9-11] Because many oxides have very high melting temperatures, the thermal stability of ceramic anodes is likely to be good. Unfortunately, the electrochemical performance of fuel cells based on ceramic anodes tends to be poor due to the fact that few oxides exhibit good electronic conductivities at the highly reducing conditions present in SOFC anodes.[8] The oxides that do show reasonably good conductivity under these conditions exhibit poor ionic conductivity and catalytic activity.

Anode performance comparable to that observed with Ni–YSZ composites has recently been observed in an electrode for which the functional layer was prepared by infiltration of $La_{0.8}Sr_{0.2}Cr_{0.5}Mn_{0.5}O_3$ (LSCM) and catalytic amounts of Pd (0.5 wt %) and ceria (5 wt %) into porous YSZ.[12] These composite electrodes have electronic conductivity due to LSCM, ionic conductivity due to the YSZ scaffold, and catalytic activity due to the Pd/ceria. An SOFC with this anode exhibited maximum power densities at 1073 K of 1.1 W/cm^2 in H_2 and 0.71 W/cm^2 in methane. An especially interesting feature of these electrodes is their relatively high electronic conductivity. Although the intrinsic conductivity of LSCM in humidified H_2 is only between 1 and 2 S/cm at 1173 K,[13] the 45 wt % LSCM–YSZ composite, for which the LSCM phase was only 30 vol % of the solid, exhibited a conductivity greater than 0.1 S/cm at this temperature. (A conductivity of 0.1 S/cm is sufficient for the functional layer of an electrode, so long as a conduction layer is present for lateral conduction.[14]) A random composite consisting of only 30 vol % of the conductive phase would normally have a conductivity much less than 20 times that of the conductive phase; however, the nonrandom nature of the composite leads to a much higher conductivity than expected.[15]

Under reducing conditions, oxides based on the doping of $SrTiO_3$ exhibit some of the highest conductivities among ceramics.[16-21] In particular, $La_{0.3}Sr_{0.7}TiO_3$ (LST) has been reported to have conductivities greater than 20 S/cm at 1173 K under anode conditions.[22] LST does not undergo solid state reactions with YSZ, even after calcination at 1823 K.[23] Modest success has been reported with SOFC anodes that were conventional composites of LST and ceria,[24,25] but the reported anode overpotentials and fuel cell power densities were clearly not comparable to that achieved with the best Ni–YSZ anodes. In a study from our laboratory, SOFC anodes were prepared by infiltrating a Pd/ceria catalyst into a porous scaffold that was itself a composite of LST and YSZ.[26] Again, the performance of these electrodes was only modest. Furthermore, the conductivities of composites with 35 vol % LST were only 0.1 S/cm at 1173 in humidified H_2, a factor of more than 200 lower than the value reported for bulk LST.

Because structure seems to play a large role in the performance of the infiltrated-LSCM electrodes, and because LSCM is required primarily for its electronic conductivity,[12] it is interesting to consider whether infiltrated-LST electrodes might perform even better, due to the higher electronic conductivity of LST. Furthermore, because LST is less reactive with YSZ than is LSCM, a wider range of processing conditions can be used for these materials. However, we will show in this paper that the structure of the infiltrated LST is very different from that of the LSCM, possibly because of weaker surface interactions. These structural differences lead to the compos-

* Electrochemical Society Active Member.
z E-mail: gorte@seas.upenn.edu

ites exhibiting a lower conductivity than expected. Also, while the performance of the LST-based electrodes is reasonable, it is not comparable to that achieved with LSCM.

Experimental

As in the previous study with LSCM, cells were fabricated from a three-layer YSZ wafer with two porous layers separated by a 60 μm thick, dense electrolyte layer.[12] The three-layer YSZ wafers were produced by laminating three green tapes, synthesized by tape casting, with pore formers in the two outer layers. The laminated green tapes were fired to 1773 K to produce the final structures. The porous layer on one side of the electrolyte was 200 μm thick YSZ (~65% porous) and was used as the scaffold for the cathodes, while the other porous layer was 50 μm thick YSZ (~65% porous) and was used as the scaffold for the anode. Porosity in both layers was obtained using graphite as a pore former.[27-29]

After synthesizing the three-layer YSZ wafer, LST was added to the porous anode layer by infiltration of an aqueous solution of the metal salts. For this study, the LST content was fixed at 45 wt %, or 35 vol %, of the anode. (Note: The compositions in this paper are based on the total weight and volume of the electrode.) The aqueous solution was prepared from $La(NO_3)_3 \cdot 6H_2O$ (Alfa Aesar, ACS 99.9%), $Sr(NO_3)_2$ (Alfa Aesar, ACS 99.0%), $[CH_3CH(O\text{-})CO_2 \cdot NH_4]_2 \cdot Ti(OH)_2$ [dihydroxy-bis-ammonium, lactate, titanium (IV), Alfa Aesar], and distilled water in the correct molar ratios. After infiltrating the porous layer with this solution, the wafer was heated in air to 723 K to decompose volatile materials. The procedure was repeated approximately 15 times until the desired weight loading of LST was achieved. Finally, the wafer was calcined in air between 1373 and 1573 K for 4 h to produce the perovskite structure.

After forming the LST in the anode layer, the LSF ($La_{0.8}Sr_{0.2}FeO_3$)–YSZ cathodes were synthesized by impregnating the 200 μm thick layer with an aqueous solution containing $La(NO_3)_3 \cdot 6H_2O$, $Sr(NO_3)_2$, and $Fe(NO_3)_3 \cdot 9H_2O$, to a loading of 40 wt % (~25 vol %) LSF, followed by calcination to 1123 K. Detailed procedures for forming the LSF–YSZ cathodes and a complete description of their characteristics are given elsewhere.[30,31] Based on those studies, the impedance at 973 K of LSF–YSZ cathodes prepared in this way is between 0.1 and 0.15 Ω cm^2 and is independent of current density. Following the addition of LSF, 0.5 wt % (~0.2 vol %) Pd and 5 wt % (~3 vol %) ceria were added as catalysts to the anode layer in most of the cells by infiltration of aqueous solutions of the nitrate salts and heating in air to 723 K.

The electronic conductivities of the LST–YSZ composites were measured as a function of temperature in humidified (3% H_2O) H_2, using four-probe measurements, on samples that were prepared by infiltrating 45 wt % (~35 vol %) LST into porous YSZ slabs that were 2.5 × 2.5 × 10 mm in size. The YSZ slabs were prepared by lamination and sintering of the same green tapes used for the preparation of the electrode layer. Because the electronic conductivity of LST in reducing environments shows hysteresis with temperature and $P(O_2)$,[25] the measurements in our study were first performed in humidified (3% H_2O) H_2 with increasing temperature, on a sample that had initially been calcined in air, then again with decreasing temperature.

For fuel cell testing, cells were attached to a 10 mm diameter alumina tube with a ceramic adhesive (Aremco, Ceramabond 552). Electrical connections were achieved using Ag paste and Ag wire at both the anode and cathode. The fuel to the anode was humidified (3% H_2O) H_2 with a flow rate of 50 mL/min and injected within a distance of 30 mm from the anode surface using a 3 mm diameter tube, while the cathode was exposed to air. Impedance spectra were measured at open circuit in the galvanostatic mode with a frequency range of 0.1 Hz to 100 kHz and a 1 mA root-mean-square ac perturbation using a Gamry Instruments potentiostat. The active area of the cells, equal to the anode area, was 0.35 cm^2, but the area of the electrolyte and cathode was approximately 1 cm^2.

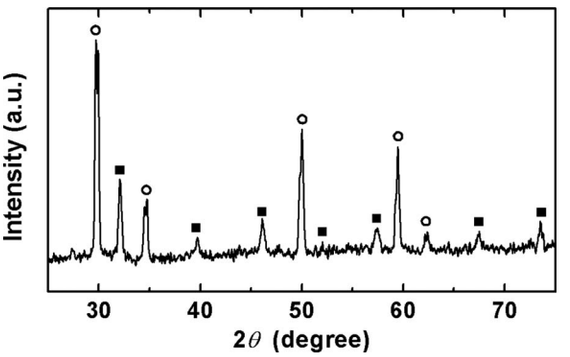

Figure 1. XRD pattern of the 45 wt % LST–YSZ composite that had been calcined to 1473 K. YSZ (○) and LST (■).

Results

Physical characterization of the LST–YSZ composites.— To determine the structure of the infiltrated LST–YSZ composites, the materials were characterized by X-ray diffraction (XRD) and scanning electron microscopy (SEM). Figure 1 is a diffraction pattern of the composite, performed on a 50 μm thick slab that had been calcined to 1473 K. The pattern demonstrates that the composite has the proper microstructure, because the primary diffraction lines were those corresponding to the LST and YSZ phases.

SEM micrographs of LST–YSZ composites are shown in Fig. 2. Figure 2a shows the porous YSZ structure prior to the addition of LST and indicates that YSZ is made up of random pores, ranging between 1 and 10 μm in size. Previous Brunauer, Emmett, and Teller surface-area measurements indicated a specific surface area of 0.4 m^2/g,[32] demonstrating that the YSZ scaffold must be essentially dense, with no significant microporosity. Figure 2b is the micrograph obtained following the addition of 45 wt % LST and calcination to 1373 K. The figure demonstrates that the open structure of the YSZ has now been filled with small LST particles, approximately 0.1 μm in size. While the LST particles are in contact with each other, they are loosely packed, so that the porosity of LST phase within the YSZ pores is roughly 50%. Because the porosity of the YSZ prior to the addition of LST was approximately 65%, the total volume percent of LST in the LST–YSZ composite is estimated to be 30 vol % based on the SEM results, close to the value of 35 vol % calculated from the weight loading. Figure 2c shows the same LST deposits at higher magnification, with the YSZ scaffold at the bottom.

Figures 2d and e are micrographs at low and high magnification of the LST–YSZ composites after calcination to 1573 K. Although previous work has demonstrated that there are no solid state reactions between LST and YSZ at temperatures up to at least 1823 K,[23] calcination to the higher temperature resulted in significant sintering of the LST within the YSZ pores. The feature size of the LST in the center of the pores has increased to approximately 0.5 μm. Even more important, a significant fraction of the LST appears to have collapsed onto the surface of the YSZ pores. This is especially observable in Fig. 2e, which suggests there is a rough coating of LST over the YSZ scaffold.

The conductivities of the 45 wt % LST–YSZ composite in humidified (3% H_2O) H_2, determined using four-probe measurements, are shown as a function of temperature in Fig. 3. Because the conductivity of the porous YSZ was very low compared to any of the values shown in Fig. 3,[12] the conductivities are due to the LST incorporated in the pores. The same sample was used in each of the three sets of data reported in the figure, but the sample was initially

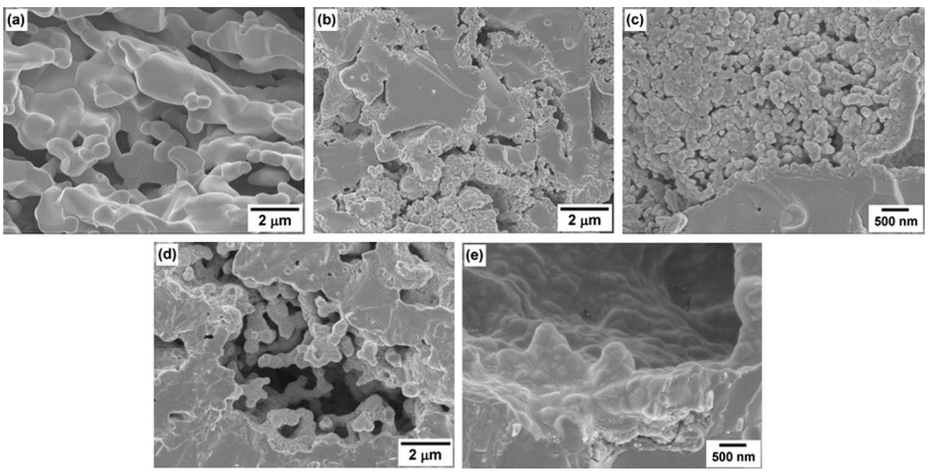

Figure 2. Scanning electron micrographs of (a) the porous YSZ backbone prior to the addition of LST, (b) the 45 wt % LST–YSZ composite calcined to 1373 K (lower magnification), (c) the 45 wt % LST–YSZ composite calcined to 1373 K (higher magnification), (d) the 45 wt % LST–YSZ composite calcined to 1573 K (lower magnification), and (e) the 45 wt % LST–YSZ composite calcined to 1573 K (higher magnification).

calcined to only 1373 K for the first set, then 1473 K, and finally 1573 K. The conductivities were measured while increasing the temperature of the sample and again while decreasing the temperature. As reported by others,[25] the conductivities increased significantly with increasing reduction temperatures but remained relatively constant when cooling in a reducing environment.

Two observations are made from the data in Fig. 3. First, the conductivities of the composite decreased substantially with increasing calcination temperature, with the 1573 K composite exhibiting conductivities that were approximately 5 times lower than that of the 1373 K composite. Second, the conductivity of the composite calcined at 1373 K and reduced at 1173 K was greater than 0.4 S/cm, a value higher than was achieved by more traditional LST–YSZ composites having higher volume fractions of LST.[26] The obvious conclusion is that the structure of the composite is important in determining the conductivity, and that the structural changes that occur with increasing calcination temperature cause a decrease in the conductivity.

Electrochemical characterization of LST–YSZ composites.— Figure 4 shows the polarization curves for two fuel cells, operating in humidified (3% H_2O) H_2 at 1073 K, for which the anode was made from the 45 wt % LST–YSZ composite that had been calcined to 1373 K. Both cells had identical LSF–YSZ cathodes and 60 μm thick electrolytes, and differed only in that 5 wt % ceria and 0.5 wt % Pd had been added to one of the cells for catalytic activity. While the open-circuit voltages (OCVs) were approximately 1.1 V for both cells, in good agreement with the Nernst potential, the addition of the catalyst had a dramatic effect on fuel cell performance. The maximum power density increased from less than 20 to approximately 780 mW/cm^2 upon the addition of Pd/ceria, demonstrating that LST itself has minimal electrochemical activity for oxidation of H_2.

Additional characteristics of the 1373 K, LST–YSZ anode, with the Pd/ceria catalyst, are demonstrated in Fig. 5 and 6, which show the *V-i* polarization and Cole–Cole impedance plots as a function of temperature in humidified H_2. The *V-i* polarization curves in Fig. 5 indicate that the cell potentials decrease linearly with the current density. As expected, the maximum power densities increased with temperature, from 400 mW/cm^2 at 973 K to 1100 mW/cm^2 at 1173 K.

The sources of the losses in the fuel cell were investigated using the open-circuit impedance plots in Fig. 6. The ohmic losses, determined by the high-frequency intercept with the abscissa, decrease

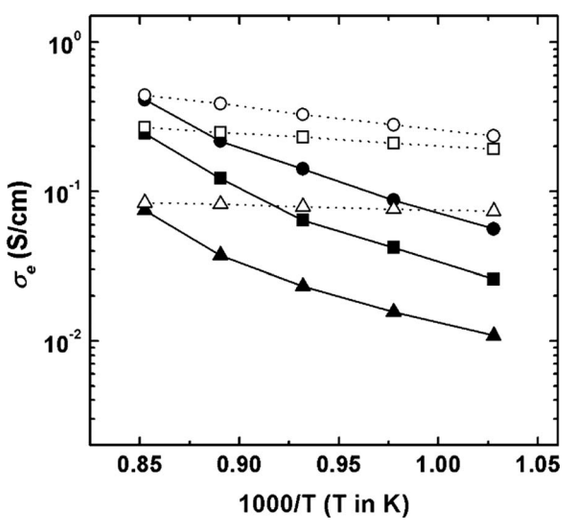

Figure 3. Electrical conductivity of the 45 wt % LST–YSZ composite in humidified (3% H_2O) H_2 as a function of temperature. Data were obtained (●) on heating and (○) on cooling for the sample calcined to 1373 K, (■) on heating and (□) on cooling for the sample calcined to 1473 K, (▲) on heating and (△) on cooling for the sample calcined to 1573 K.

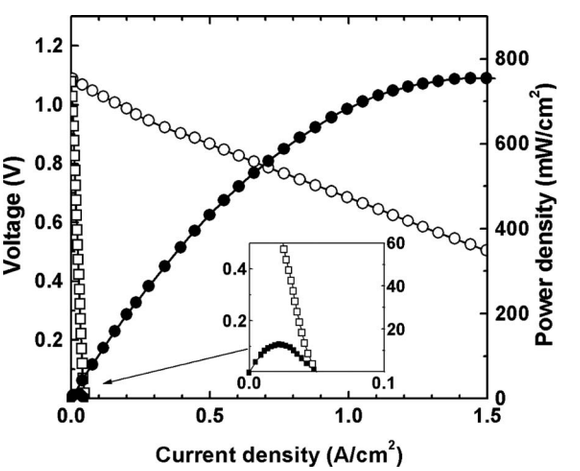

Figure 4. *V-i* polarization curves for the cells having an anode with 45 wt % LST, 5 wt % ceria, and 0.5 wt % Pd (○ designates *V* and ● power density) and with only 45 wt % LST (□ designates *V* and ■ power density). The data were obtained in humidified (3% H_2O) H_2 at 1073 K.

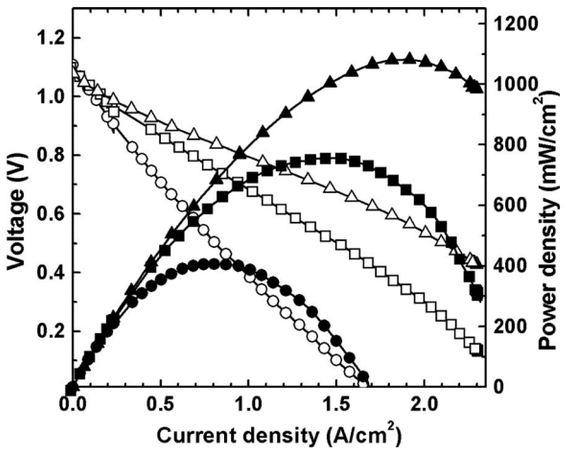

Figure 5. *V-i* polarization curves for cells with 45 wt % LST calcined at 1373 K, with 5 wt % ceria and 0.5 wt % Pd, in humidified (3% H_2O) H_2 at 973 K (○ shows *V* and ● power density), 1073 K (□ designates *V* and ■ power density), 1073 K, and 1173 K (△ designates *V* and ▲ power density).

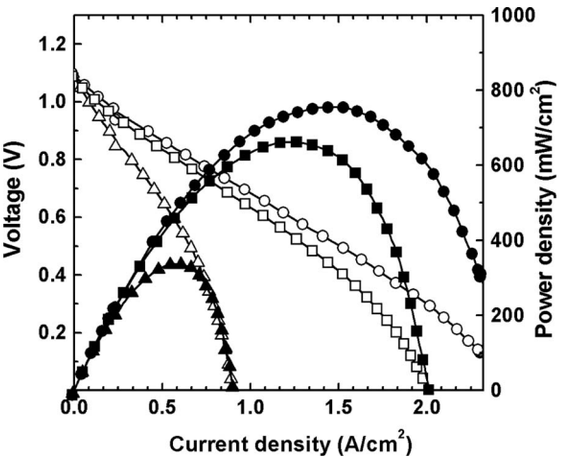

Figure 7. *V-i* polarization curves for the cells having an anode with 45 wt % LST, 5 wt % ceria, and 0.5 wt % Pd, in humidified H_2 at 1073 K. The LST was calcined to either 1373 K (○ designates *V* and ● power density), 1473 K (□ designates *V* and ■ power density), or 1573 K (△ designates *V* and ▲ power density).

from 0.42 Ω cm^2 at 973 K to 0.12 Ω cm^2 at 1173 K. The ohmic loss at 973 K is 0.07 Ω cm^2 higher than the value calculated for a 60 μm thick YSZ electrolyte, 0.35 Ω cm^2.[33] However, because the conductivity, shown in Fig. 3, of the LST–YSZ composite at 973 K is only 0.06 S/cm prior to high-temperature treatment, calculations suggest the 50 μm thick anode should contribute 0.08 Ω cm^2 to the ohmic losses at this temperature, a value very close to the difference between the observed ohmic losses and expected electrolyte losses. The conductivity of the LST–YSZ composite is sufficient to make the ohmic losses negligible at higher temperatures.

At all temperatures investigated, the majority of the cell losses is nonohmic, as determined from the distance between the low- and high-frequency intercepts with the abscissa. Assuming the losses associated with the LSF–YSZ cathode are approximately 0.1 Ω cm^2 at 973 K,[30] the anode losses are estimated to be 0.6 Ω cm^2 at this temperature. Because there is some curvature in the *V-i* curve at OCV, this overstates the actual anode losses somewhat. Using the average slope of the *V-i* curve at 973 K between 1.1 and 0.5 V, the total area-specific resistance of the cell was determined to be 0.8 Ω cm^2, so that the average anode losses must be closer to 0.3 Ω cm^2. At 1173 K, the nonohmic impedance at OCV was approximately 0.45 Ω cm^2 based on the data in Fig. 6, but, because the average slope of the *V-i* curve is only 0.29 Ω cm^2 at this temperature, the average anode losses must be less than 0.2 Ω cm^2.

To investigate how the structural changes observed in Fig. 2 affect electrode performance, we prepared three fuel cells that were identical except for the LST–YSZ calcination temperatures, which were 1373, 1473, and 1573 K. The anodes in these cells again contained 0.5 wt % Pd and 5 wt % ceria, added after the LST was calcined. The *V-i* polarization curves and open-circuit Cole–Cole impedance plots, obtained in humidified H_2 at 1073 K, are shown in Fig. 7 and 8. The data indicate that there is a continuous decrease in the performance of the cell with increasing LST calcination temperature. Some of this decrease is due to a loss of conductivity. According to Fig. 3, the 1573 K LST–YSZ composite has a conductivity of only 0.025 S/cm at 1073 K, so the resistance of the 50 μm anode should be 0.2 Ω cm^2. Adding this to the expected resistance of the 60 μm YSZ electrolyte, 0.15 Ω cm^2, the total ohmic losses should be 0.35 Ω cm^2, very close to what is observed in Fig. 8. The ohmic losses for the 1373 and 1473 K cells were much closer to the value expected for the electrolyte.

However, the effect of LST–YSZ calcination temperature on the nonohmic losses was much larger. Not only was there a significant increase in the OCV impedance in Fig. 8, but the *V-i* polarization curves for the cells prepared from the 1473 and 1573 K LST–YSZ composites show an increased slope at higher current densities. This kind of behavior is often associated with gas-phase diffusion limitations, but this is not likely the cause in the present case. The pore volumes for the 1473 and 1573 K LST–YSZ composites are more open for gas-phase diffusion than that for the 1373 K composite, so that diffusion should be less limiting on the cells with the poorest performance. Based on the SEM micrographs in Fig. 2, we suggest that increased nonohmic losses are associated with the LST covering the YSZ pores, as observed in Fig. 2e. Because LST has a low ionic conductivity, the electrochemical reactions can only occur on the

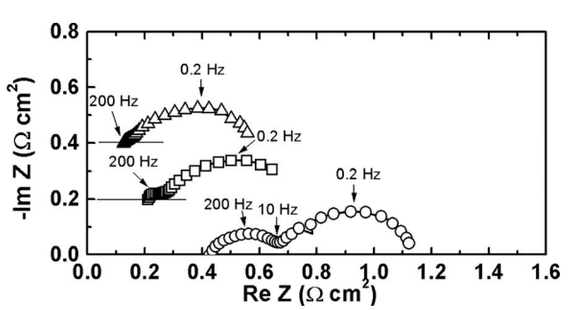

Figure 6. Cole–Cole plots for the cells with 45 wt % LST calcined to 1373 K, with 5 wt % ceria and 0.5 wt % Pd. The measurements were performed in humidified (3% H_2O) H_2 at (○) 973, (□) 1073, and (△) 1173 K.

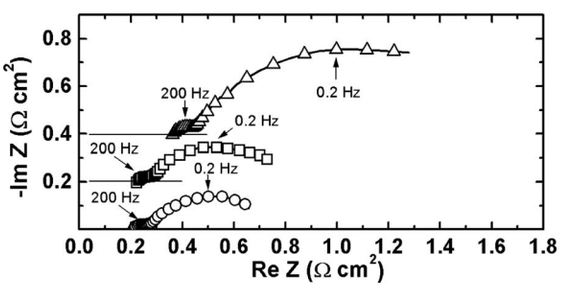

Figure 8. Cole–Cole plots for the cells with 45 wt % LST calcined, 5 wt % ceria, and 0.5 wt % Pd. The measurements were performed in humidified (3% H_2O) H_2 at 1073 K. The LST had been calcined to either (○) 1373, (□) 1473, or (△) 1573 K.

uncovered YSZ regions, decreasing the area where the three-phase boundary sites exist. Why this would cause the impedance to change with current density is uncertain.

Discussion

As pointed out earlier, LST and YSZ are completely unreactive following calcination to temperatures as high as 1823 K. In addition to the fact that LST and YSZ remain as separate phases in cofired powders, the surface interactions between these two phases are very weak, to the point that it is difficult to form ceramic structures with a sharp LST–YSZ interface because of the tendency of the two layers to delaminate.[23] This is in sharp contrast to what is observed with $La_{0.8}Sr_{0.2}MnO_3$ (LSM) and YSZ, where LSM particles have been shown to spread out over YSZ surfaces under some conditions, at temperatures below that at which solid state reactions between LSM and YSZ begin to occur.[34] These surface interactions are related to the "wetting" and "dewetting" phenomena observed with liquid–solid interfaces.

Surface interactions appear to have an important influence on the nature of composites formed by infiltration processes. In a recent study of LSCM–YSZ composites,[12] it was reported that the LSCM forms an even coating over the YSZ pores following calcination at 1473 K. Assuming that LSCM interacts with YSZ in a similar way as LSM interacts, it would appear that the tendency of the LSCM to "wet" the YSZ surface leads to a composite in which the LSCM coats the YSZ. By contrast, the tendency of LST to avoid wetting the YSZ leads to the formation of LST particles in the open channels of the structure.

We compared the fuel cell results obtained with LST–YSZ composites to those reported previously with LSCM–YSZ composites.[12] The YSZ scaffolds were identical in the two studies, and both studies incorporated 45 wt % of the infiltrated oxide. Both studies found that the electrode performance was poor unless a catalyst, Pd/ceria in both cases, was added to the composite, suggesting that the LST and LSCM act primarily as electronic conductors. The conductivity of the 1373 K LST–YSZ composite was somewhat higher than that of the LSCM–YSZ composite, at least after high-temperature reduction. However, the electrochemical performance of the LSCM–YSZ electrode was significantly better than any of the LST–YSZ electrodes. Using the same cathode material (i.e., 40 wt % LSF infiltrated into YSZ) and a similar electrolyte thickness, the cells with LSCM gave maximum power densities in humidified H_2 of 520 mW/cm^2 at 973 K and 1100 mW/cm^2 at 1073 K, compared to values of 400 and 780 mW/cm^2 on the best LST cell. At 973 K, the total nonohmic impedance of the LSCM cell, including cathode losses, was 0.2 Ω cm^2, while the anode impedance for the best 1373 K LST cell was estimated to be 0.6 Ω cm^2.

There are several possible reasons for why the LSCM-based electrode showed better performance. While the ionic conductivity of LSCM is very low under oxidizing conditions,[35] its ionic conductivity under reducing conditions is significantly better and much higher than that of LST. Another important factor is the morphology of the LSCM deposits. While the LSCM film that forms over the YSZ pore structure is not likely to be ideal, it has been observed that the LSCM film develops pores under reducing conditions, much like what is observed with LSM.[36] Under anode conditions, it is likely that the LSCM exists as a film with pores, forming an almost ideal anode structure.

Finally, it was possible in the present study to examine the properties of LST–YSZ composites while varying the morphology of the LST within the YSZ pores, simply by changing the calcination temperature. The data showed that the morphology had a significant effect on both the conductivity of the composite and on the electrochemical properties of electrodes made from this composite. The fact that morphology has such an important influence on properties is not surprising, but it does point out the critical importance that structure, separate from composition, has on the development of electrodes. This is a critical factor in reproducing results between laboratories, because the preparation methods and calcination temperatures can be just as important as the composition in determining the performance of electrodes.

Conclusions

The properties of LST–YSZ composites depend strongly on the structure of those composites. When the composites are prepared by infiltration of LST into porous YSZ, the structure of the LST phase is influenced by the surface interactions between LST and YSZ and depends on the calcination temperature. LST–YSZ composites have insufficient catalytic activity for SOFC anodes but can provide the electronic conductivity required for the functional layer.

Acknowledgments

This work was funded by the U.S. Department of Energy's Hydrogen Fuel Initiative (grant no. DE-FG02-05ER15721). S. L. acknowledges support from the Korea Research Foundation Grant, funded by the Korean Government (MOEHRD) (KRF-2007-611-D00014).

University of Pennsylvania assisted in meeting the publication costs of this article.

References

1. S. McIntosh and R. J. Gorte, *Chem. Rev. (Washington, D.C.)*, **104**, 4845 (2004).
2. N. Q. Minh, *J. Am. Ceram. Soc.*, **76**, 563 (1993).
3. C. H. Toh, P. R. Munroe, D. J. Young, and K. Foger, *Mater. High. Temp.*, **20**, 129 (2003).
4. H. Kim, C. Lu, W. L. Worrell, J. M. Vohs, and R. J. Gorte, *J. Electrochem. Soc.*, **149**, A247 (2002).
5. S. Park, J. M. Vohs, and R. J. Gorte, *Nature (London)*, **404**, 265 (2000).
6. M. D. Gross, J. M. Vohs, and R. J. Gorte, *J. Mater. Chem.*, **17**, 3071 (2007).
7. S. W. Jung, C. Lu, H. P. He, K. Ahn, R. J. Gorte, and J. M. Vohs, *J. Power Sources*, **154**, 42 (2006).
8. A. Atkinson, S. Barnett, R. J. Gorte, J. T. S. Irvine, A. J. McEvoy, M. B. Mogensen, S. Singhal, and J. Vohs, *Nat. Mater.*, **3**, 17 (2004).
9. R. T. K. Baker, M. A. Barber, P. S. Harris, F. D. Feates, and R. J. Waite, *J. Catal.*, **26**, 51 (1972).
10. R. T. Baker, P. S. Harris, J. Henderson, and R. B. Thomas, *Carbon*, **13**, 17 (1975).
11. R. T. K. Baker, P. S. Harris, and S. Terry, *Nature (London)*, **253**, 37 (1975).
12. G. Kim, G. Corre, J. T. S. Irvine, J. M. Vohs, and R. J. Gorte, *Electrochem. Solid-State Lett.*, **11**, B16 (2008).
13. S. W. Tao and J. T. S. Irvine, *J. Electrochem. Soc.*, **151**, A252 (2004).
14. M. D. Gross, J. M. Vohs, and R. J. Gorte, *Electrochem. Solid-State Lett.*, **10**, B65 (2007).
15. H. P. He, Y. Y. Huang, J. Regal, M. Boaro, J. M. Vohs, and R. J. Gorte, *J. Am. Ceram. Soc.*, **87**, 331 (2004).
16. Q. Fu, F. Tietz, D. Sebold, S. Tao, and J. T. S. Irvine, *J. Power Sources*, **171**, 663 (2007).
17. S. Koutcheiko, Y. Yoo, A. Petric, and I. Davidson, *Ceram. Int.*, **32**, 67 (2006).
18. P. Blennow, K. K. Hansen, L. R. Wallenberg, and M. Mogensen, *Electrochim. Acta*, **52**, 1651 (2006).
19. L. Yang, L. C. De Jonghe, C. P. Jacobson, and S. J. Visco, *J. Electrochem. Soc.*, **154**, B949 (2007).
20. X. Li, H. Zhao, W. Shen, F. Gao, X. Huang, Y. Li, and Z. Zhu, *J. Power Sources*, **166**, 47 (2007).
21. H. Kurokawa, L. Yang, C. P. Jacobson, L. C. De Jonghe, and S. J. Visco, *J. Power Sources*, **164**, 510 (2007).
22. T. Kolodiazhnyi and A. Petric, *J. Electroceram.*, **15**, 5 (2005).
23. K. Ahn, S. Jung, J. M. Vohs, and R. J. Gorte, *Ceram. Int.*, **33**, 1065 (2007).
24. O. A. Marina, N. L. Canfield, and J. W. Stevenson, *Solid State Ionics*, **149**, 21 (2002).
25. J. Canales-Vazquez, S. W. Tao, and J. T. S. Irvine, *Solid State Ionics*, **159**, 159 (2003).
26. G. Kim, M. D. Gross, W. S. Wang, J. M. Vohs, and R. J. Gorte, *J. Electrochem. Soc.*, **155**, B360 (2008).
27. S. Park, R. J. Gorte, and J. M. Vohs, *J. Electrochem. Soc.*, **148**, A443 (2001).
28. R. J. Gorte, S. Park, J. M. Vohs, and C. Wang, *Adv. Mater. (Weinheim, Ger.)*, **19**, 1465 (2000).
29. M. Boaro, J. M. Vohs, and R. J. Gorte, *J. Am. Ceram. Soc.*, **86**, 395 (2003).
30. Y. Huang, J. M. Vohs, and R. J. Gorte, *J. Electrochem. Soc.*, **151**, A646 (2004).
31. W. Wang, M. D. Gross, J. M. Vohs, and R. J. Gorte, *J. Electrochem. Soc.*, **154**, B439 (2007).
32. F. Bidrawn, S. Lee, J. M. Vohs, and R. J. Gorte, *J. Electrochem. Soc.*, **155**, B660 (2008).
33. K. Sasaki and J. Maier, *Solid State Ionics*, **134**, 303 (2000).
34. Y. Huang, J. M. Vohs, and R. J. Gorte, *Electrochem. Solid-State Lett.*, **9**, A237 (2006).
35. V. V. Kharton, E. V. Tsipis, I. P. Marozau, A. P. Viskup, J. R. Frade, and J. T. S. Irvine, *Solid State Ionics*, **178**, 101 (2007).
36. G. Corre, G. Kim, J. T. S. Irvine, J. M. Vohs, and R. J. Gorte, To be published.